

Evolution-inspired design of multicolored photoswitches from a single cyanobacteriochrome scaffold

メタデータ	言語: en 出版者: National Academy of Sciences 公開日: 2020-07-06 キーワード (Ja): キーワード (En): 作成者: Fushimi, Keiji, Hasegawa, Masumi, Ito, Takeru, Rockwell, Nathan C., Enomoto, Gen, -Win, Ni-Ni, Lagarias, J. Clark, Ikeuchi, Masahiko, Narikawa, Rei メールアドレス: 所属:
URL	http://hdl.handle.net/10297/00027549

1 **Title**

2 **Evolution-inspired design of multicolored photoswitches from a single**
3 **cyanobacteriochrome scaffold**

4

5 Keiji Fushimi^{a,b,1}, Masumi Hasegawa^a, Takeru Ito^a, Nathan C. Rockwell^c, Gen Enomoto^{b,d},
6 Ni-Ni-Win^d, J. Clark Lagarias^c, Masahiko Ikeuchi^{b,d}, Rei Narikawa^{a,b,e,1}

7

8 ^aGraduate School of Integrated Science and Technology, Shizuoka University, 836 Ohya,
9 Suruga, Shizuoka 422-8529, Japan

10 ^bCore Research for Evolutional Science and Technology, Japan Science and Technology
11 Agency, 4-1-8 Honcho, Kawaguchi, Saitama 332-0012, Japan

12 ^cDepartment of Molecular and Cellular Biology, University of California, Davis, California
13 95616, United States

14 ^dGraduate School of Arts and Sciences, University of Tokyo, 3-8-1 Komaba, Meguro, Tokyo
15 153-8902, Japan

16 ^eResearch Institute of Green Science and Technology, Shizuoka University, 836 Ohya,
17 Suruga, Shizuoka 422-8529, Japan

18

19 ¹To whom correspondence should be addressed.

20 Email: fushimi.keiji@shizuoka.ac.jp, narikawa.rei@shizuoka.ac.jp, Tel: +81-54-238-4783

21

22 **Keywords**

23 broadband spectrum, photoconversion, color-tuning, optogenetics

24

25

26 **Abstract**

27 Cyanobacteriochromes (CBCRs) are small, bistable linear tetrapyrrole (bilin)-binding light
28 sensors which are typically found as modular components in multi-domain cyanobacterial
29 signaling proteins. The CBCR family has been categorized into many lineages that roughly
30 correlate with their spectral diversity, but CBCRs possessing a conserved DXCF motif are
31 found in multiple lineages. DXCF CBCRs typically possess two conserved Cys residues: a
32 first Cys that remains ligated to the bilin chromophore, and a second Cys found in the DXCF
33 motif. The second Cys often forms a second thioether linkage, providing a mechanism to
34 sense blue and violet light. DXCF CBCRs have been described with blue/green, blue/orange,
35 blue/teal and green/teal photocycles, and the molecular basis for some of this spectral
36 diversity has been well established. We here characterize AM1_1499g1, an atypical DXCF
37 CBCR that lacks the 2nd cysteine residue and exhibits an orange/green photocycle. Based on
38 prior studies of CBCR spectral tuning, we have successfully engineered seven new
39 AM1_1499g1 variants that exhibit robust yellow/teal, green/teal, blue/teal, orange/yellow,
40 yellow/green, green/green, and blue/green photocycles. The remarkable spectral diversity
41 generated by modification of a single CBCR provides a good template for multiplexing
42 synthetic photobiology systems within the same cellular context, thereby bypassing the time-
43 consuming empirical optimization process needed for multiple probes with different protein
44 scaffolds.

45

46 **Significance statement**

47 Cyanobacteriochromes (CBCRs) are small cyanobacterial photoreceptors which are highly
48 diversified and categorized into many lineages based on their primary sequences. In this
49 study, we identified an atypical CBCR exhibiting an orange/green reversible photocycle.
50 Step-by-step site-directed mutagenesis was performed on this native CBCR, and seven new
51 photoconvertible variants were created. During this process, we identified residues crucial for
52 each color tuning event. These seven molecules covering the shorter wavelength blue-to-
53 orange region would contribute to the future development of multi-colored optogenetic tools
54 and are complementary to recently developed molecules sensing longer wavelengths of light.

55

56 **Introduction**

57 Cyanobacteriochromes (CBCRs) are single-domain light sensors that incorporate linear
58 tetrapyrrole (bilin) chromophores such as phycoviolobin (PVB) and phycocyanobilin (PCB)
59 (*SI Appendix*, Fig. S1 A and B) (1, 2). Like the distantly related phytochromes, CBCRs are
60 covalently bound to their bilins via a thioether linkage between a conserved ‘1st Cys’ (ore
61 ‘canonical’ Cys) and the C3 side chain of the bilin. Both CBCRs and canonical phytochromes
62 (3) use photoisomerization of the C15–C16 bilin double bond to trigger reversible
63 photoconversion between their *15Z* dark state and their *15E* photoproduct state via a series of
64 intermediates (*SI Appendix*, Fig. S1 A and B).

65 CBCRs exhibit a broad spectral range of photocycles from the ultraviolet to the far-red,
66 and the molecular basis of their light-sensing properties has been extensively studied by
67 spectroscopic and structural methods (2). A number of different CBCR subfamilies have been
68 identified by primary sequence and phylogenetic analysis, and these subfamilies often exhibit
69 different photocycles. Multiple CBCR lineages contain a highly conserved Asp-Xaa-Cys-Phe
70 (DXCF) signature sequence roughly corresponding to a conserved Asp-containing motif in
71 phytochromes (corresponding to Asp207 in the model phytochrome Cph1) (4). This motif
72 provides DXCF CBCRs with a second conserved Cys residue or ‘2nd Cys’ that plays a
73 critical role in spectral tuning of these proteins (5–11).

74 ‘Prototypical’ DXCF CBCRs initially incorporate PCB as chromophore precursor and
75 then isomerize it to PVB over time to yield photoreceptors with blue-absorbing (*^{15Z}Pb*) dark
76 states and green-absorbing (*^{15E}Pg*) photoproduct states (a blue/green photocycle; Fig. 1 A and
77 B and *SI Appendix*, Figs. S1C and S2 A and B) (5, 9, 11–15). Several studies have established
78 that the secondary structures of the protein scaffold, especially near the DXCF motif, are
79 dynamically changed upon photoconversion (Fig. 1C and *SI Appendix*, Fig. S2 A and B) (16–
80 18). The 2nd Cys residue contributes to two important processes, i.e. PCB-to-PVB

81 isomerization and reversible thioether linkage formation at the C10 position of the
82 chromophore during the photoconversion cycle (5, 7, 14). Both processes shorten the π -
83 conjugated system and strongly blue shift the absorption of the bound chromophore into the
84 blue and violet range (*SI Appendix*, Figs. S1 A and B and S2 A and B).

85 Other DXCF CBCRs are unable to catalyze the PCB-to-PVB chromophore conversion
86 or to form linkages with the 2nd Cys residue (Fig. 1D and *SI Appendix*, Fig. S2C) (8, 9, 11,
87 15, 19, 20). Those unable to generate PVB exhibit blue/yellow or blue/orange photocycles
88 instead of the prototypical blue/green DXCF CBCR photocycle (*SI Appendix*, Fig. S1D). This
89 arises from the reversible photoconversion between their dual cysteine-linked 15E Pb dark
90 states and yellow-absorbing (15E Py) (or orange-absorbing (15E Po)) photoproduct states that
91 are red shifted from those of photoproduct states of DXCF CBCRs with PVB chromophores
92 (*SI Appendix*, Fig. S2C-i). DXCF CBCRs that lack the 2nd linkage retain the fully
93 conjugated π -systems in both dark and photoproduct states, which can absorb in the teal-to-
94 yellow region with PVB (*SI Appendix*, Fig. S2C-ii).

95 In addition to PCB-to-PVB isomerization and second linkage formation, spectral blue
96 shifting can also occur via a ‘trapped-twist’ mechanism, e.g. photoproduct states of red/green
97 CBCRs in which the chromophore’s ring D adopts a twisted geometry relative to the plane of
98 the B- and C-rings (*SI Appendix*, Fig. S2C-iii) (15, 21). DXCF CBCRs with PVB can form
99 such a photoproduct state; formation of the second linkage in such cases results in a blue/teal
100 photocycle, whereas absence of this linkage yields a green/teal photocycle (8, 11, 15, 19).
101 Thus, much of the spectral diversity of DXCF CBCR photocycles can be explained by three
102 mechanisms: i. PCB-to-PVB isomerization, ii. reversible Cys-adduct formation, and iii.
103 trapping of a twisted D-ring in the photoproduct state (*SI Appendix*, Fig. S2C).

104 Previously, we characterized a number of CBCRs from the symbiotic cyanobacterium
105 *Acaryochloris marina* MBIC11017 (8, 22–25). In the present study, we focus on a newly

106 identified member of the DXCF CBCR subfamily from *A. marina*, AM1_1499g1, that lacks
107 the 2nd Cys residue. A close relative of AM1_6305g1, AM1_1499g1 is a member of a DXCF
108 CBCR lineage that contains the previously studied CBCRs, FdDpxAg, NpR5113g1,
109 NpR1597g1 and NpR5113g3 (Fig. 1D) (8, 11, 19). Members of this class of CBCRs exhibit
110 teal-absorbing photoproducts with blue/teal (NpR1597g1 and NpR5113g3) and green/teal
111 (AM1_6305g1, FdDpxAg, and NpR5113g1) photocycles. The teal-absorbing (^{15E}Pt)
112 photoproduct states of this DXCF CBCR lineage all possess trapped-twisted PVB
113 chromophores, whereas their distinct dark state spectra reflect the ability (or inability) of the
114 2nd Cys to form the second linkage at C10. Due to the absence of a 2nd Cys, we reasoned
115 that AM1_1499g1 would possess a PCB chromophore and would exhibit a photocycle
116 distinct from that of prototypical DXCF CBCRs. The present studies establish that
117 AM1_1499g1 has an orange/green photocycle and a singly-linked PCB chromophore. We use
118 site-directed mutagenesis of AM1_1499g1, informed by amino acid sequences of other
119 members of this lineage, to experimentally reconstruct a pathway of molecular evolution that
120 recapitulates most of the broad spectral palette of DXCF-containing CBCRs.

121

122 **Results and Discussion**

123 **Wild-type AM1_1499g1 senses orange light with a PCB chromophore and exhibits**
124 **thermochromic behavior.** His-tagged AM1_1499g1 was expressed in the PCB-producing
125 *Escherichia coli* and purified using the Ni-affinity column chromatography (*SI Appendix*, Fig.
126 S3 A and B). Serendipitously, we observed a violet to blue color change of the purified
127 white-light exposed solution when the solution temperature was increased (*SI Appendix*, Fig.
128 S3A). This change reflected the shift of the absorption maximum of the photoproduct from
129 green at 5°C to orange at 30°C (*SI Appendix*, Fig. S4A). AM1_1499g1 showed reversible
130 photoconversion between an orange-absorbing ^{15Z}Po dark state ($\lambda_{max} = 613$ nm) and a green-
131 absorbing ^{15E}Pg photoproduct ($\lambda_{max} = 544$ nm) at 5°C. At 30°C, the orange-absorbing ($\lambda_{max} =$
132 618 nm) ^{15Z}Po dark state converted to a yellow-absorbing ($\lambda_{max} = 589$ nm) ^{15E}Py
133 photoproduct (Figs. 2A, 3A, Table 1, and *SI Appendix*, Fig. S4A and Table S1). No blue- or
134 violet-absorbing species were observed, consistent with the absence of the DXCF Cys in this
135 protein.

136 To test whether PVB-to-PCB isomerization is responsible for this thermochromic
137 behavior, we compared the normalized photochemical difference spectra (dark state –
138 photoproduct state) of AM1_1499g1 obtained at 5°C and 30°C before and after denaturation
139 (*SI Appendix*, Fig. S4A and Table S1). These comparisons revealed that the two difference
140 spectra were identical after denaturation, indicating that the bound chromophore was PCB for
141 the both preparations. Hence, PVB-to-PCB isomerization was not responsible for the
142 temperature-dependent photoproduct spectral shift, again consistent with the absence of the
143 second Cys residue.

144 It is possible that the temperature-dependent spectral shift of the AM1_1499g1
145 photoproduct is due to temperature-dependent pK_a s of the chromophore and/or of nearby
146 residues in the protein. However, work on the red/green CBCR NpR6012g4 has demonstrated

147 that *15E*-PCB can be protonated in the trapped-twist green-absorbing state and can adopt a
148 more relaxed orange-absorbing state (26, 27), so we favor the hypothesis that the
149 chromophores of the green- and yellow-absorbing photoproduct species correspond to
150 similarly constrained and relaxed D-ring chromophores, respectively. Formation of the more
151 relaxed species at higher temperature could indicate that the green-absorbing species is a
152 trapped intermediate, but our data suggest that the two photoproduct species are present at
153 both temperatures in varying ratios. Similar heterogeneity as a function of temperature has
154 been shown to proceed with a change in heat capacity in Cph1 (28), so it is possible that a
155 significant change in the protein structure is responsible for the interconversion between these
156 two photoproduct states as well.

157

158 **The $S_{118}C$ variant of AM1_1499g1 restores PCB-to-PVB isomerization, but not 2nd Cys**
159 **linkage formation.** AM1_1499g1 is most closely related to the green/teal DXCF CBCR,
160 AM1_6305g1, which retains the 2nd Cys residue (Fig. 1D). We previously showed that
161 AM1_6305g1 retains PCB-to-PVB isomerization activity despite its inability to form a C10
162 thiol adduct (8). We hypothesized that the introduction of the 2nd Cys into AM1_1499g1, i.e.
163 via construction of the $S_{118}C$ variant (*SI Appendix*, Fig. S3B), would confer the ability to
164 isomerize PCB into PVB. Indeed, similar to AM1_6305g1, the $S_{118}C$ variant of AM1_1499g1
165 possessed a PVB chromophore and exhibited a yellow/teal photocycle (Figs. 2B, 3A, Table 1,
166 and *SI Appendix*, Fig. S4B and Table S1). By comparison with the spectra of wild-type
167 AM1_1499g1, both forms of $S_{118}C$ possessed significantly blue-shifted absorption maxima,
168 consistent with their singly-linked PVB chromophore (*SI Appendix*, Fig. S4A and B). Taken
169 together, these results indicate that introduction of the 2nd Cys residue is sufficient to restore
170 the PCB-to-PVB isomerization activity to the $S_{118}C$ variant of AM1_1499g1 but is
171 insufficient for forming the 2nd Cys linkage.

172

173 **Exploiting known DXCF CBCR diversity to engineer color tuning of the *15Z*-dark state.**

174 The absorption maximum of the ^{15Z}Py dark state of S₁₁₈C AM1_1499g1 unexpectedly was 20
175 nm red-shifted from that of the ^{15Z}Py dark state of its closest DXCF CBCR relative,
176 AM1_6305g1 (8). By examining the TePixJg structure (16, 17), we identified Tyr151 and
177 Thr159 in AM1_1499g1, which replace Leu and Asn residues in AM1_6305g1, TePixJg, and
178 many other DXCF CBCRs (Fig. 1 A and C). To test the role of both residues on dark state
179 color tuning, we constructed these variants in the S₁₁₈C background to obtain the S₁₁₈C/Y₁₅₁L
180 and S₁₁₈C/T₁₅₉N double mutant proteins (*SI Appendix*, Fig. S5 A–C). Peaking in the yellow-
181 green region (~570 nm), the dark state absorption maxima of both variants were blue-shifted
182 by ~10 nm relative to the S₁₁₈C parent.

183 We next constructed the S₁₁₈C/Y₁₅₁L/T₁₅₉N triple mutant variant (*SI Appendix*, Fig.
184 S3B). The dark state spectrum of this variant was even further blue shifted than those of the
185 double mutants, thereby establishing that the two substitutions additively affected the color-
186 tuning of the dark state (*SI Appendix*, Fig. S5C). The resulting triple mutant variant exhibited
187 a green/teal photocycle that was nearly identical to that of AM1_6305g1 (Figs. 2C, 3A, Table
188 1, and *SI Appendix*, Fig. S4C and Table S1). Reverse engineering to introduce Tyr and Thr
189 residues into AM1_6305g1 was also performed (*SI Appendix*, Fig. S3C). The dark state
190 spectrum of the resulting AM1_6305g1_L₁₃₂Y/N₁₄₀T variant was almost identical to that of
191 AM1_1499g1 (*SI Appendix*, Fig. S6 A and B and Table S1). Taken together, these studies
192 show that both of these residues perform crucial roles for color-tuning of the dark state.

193 Based on the TePixJg structure, the side-chains of residues corresponding to Tyr151
194 and Thr159 in the AM1_1499g1_S₁₁₈C variant are located in a good position to influence the
195 D-ring geometry in the dark state (Fig. 1A and *SI Appendix*, Fig. S7A). Since the dark state of
196 the S₁₁₈C variant lacks the 2nd linkage, unlike that of TePixJg, it is difficult to predict the

197 structure and conformation of the S₁₁₈C dark state chromophore. We hypothesize that the
198 replacements of Tyr151 and Thr159 with Leu and Asn are responsible for constraining the D-
199 ring in a twisted conformation (*SI Appendix*, Fig. S7 B–D). In support of this interpretation,
200 the D-ring carbonyl of the dark-state chromophore of TePixJg appears to be constrained to an
201 out-of-plane conformation by hydrogen bonding with the side-chain of Asn535. Replacement
202 of this Asn with Thr159, as found in AM1_1499g1, would require extensive chromophore
203 repositioning to support such a hydrogen bond. Replacement of Leu with Tyr151 in
204 AM1_1499g1 also might influence the positioning of the chromophore via its ability to
205 hydrogen bond with other residues such as His177, a strongly conserved residue known to
206 constrain the D-ring in *15Z* dark states of CBCRs and phytochromes (4, 17, 29). Indeed, the
207 corresponding histidine residue in TePixJg, His553, participates in chromophore positioning
208 by also forming an H-bond to the D-ring carbonyl (16, 17).

209

210 **A conserved Tyr residue performs a critical role in second linkage formation.** We next
211 focused on identifying residues that affect reversible Cys-adduct formation. According to our
212 phylogenetic analyses, AM1_1499g1 and AM1_6305g1 are members of a CBCR lineage
213 comprised of the green/teal CBCRs, FdDpxAg and NpR5113g1, and the blue/teal CBCRs,
214 NpR1597g1 and NpR5113g3 (Fig. 1D). From a sequence alignment and structural
215 information, we identified residues conserved in the blue/teal CBCR lineage – a lineage that
216 retains the ability to form reversible 2nd Cys linkages. One of these was a Tyr residue next to
217 the 1st Cys residue that is conserved only among the blue/teal CBCR lineage (Fig. 1 A and C).
218 To determine the role of this Tyr residue in 2nd Cys linkage formation, we replaced the His
219 residue at this position in AM1_1499g1 with Tyr in the S₁₁₈C variant background to construct
220 the S₁₁₈C/H₁₄₇Y variant (*SI Appendix*, Fig. S3B). We observed that this S₁₁₈C/H₁₄₇Y variant
221 bound PVB and exhibited reversible photoconversion between a blue-absorbing ($\lambda_{\text{max}} = 414$

222 nm) ^{15Z}Pb dark state and a teal-absorbing ($\lambda_{\text{max}} = 492$ nm) ^{15E}Pt photoproduct (Figs. 2D, 3A,
223 Table 1, and *SI Appendix*, Fig. S4D and Table S1). Owing to the extremely blue-shifted dark
224 state, these studies confirm the role of Tyr147 for 2nd linkage formation in the dark state. The
225 teal-absorbing photoproduct is consistent with the lability of the 2nd linkage in this variant
226 upon photoconversion.

227 To further examine the importance of this Tyr residue for Cys-adduct formation, we
228 replaced the conserved His residue with Tyr at this position in the green/teal CBCR
229 AM1_6305g1 and conversely replaced the conserved Tyr residue with His at this position in
230 the blue/teal CBCR NpR5113g3 (*SI Appendix*, Figs. S3 C and D, S6 A and C–E, and Table
231 S1). The H₁₂₈Y variant of AM_6305g1 absorbed blue light, whereas the Y₄₈₂H variant of
232 NpR5113g3 absorbed yellow light. In each case, the teal-absorbing photoproduct state
233 spectra were almost identical to those of the wild-type parent. Fully consistent with the
234 results for AM1_1499g1, these results indicate that this His/Tyr position is a crucial
235 determinant for Cys-adduct formation. In TePixJg, this His residue is located directly above
236 rings B and C (Fig. 1 A and C and *SI Appendix*, Fig. S7A). We hypothesize that the larger
237 side chain of the Tyr residue helps to reposition the chromophore closer to the 2nd Cys
238 residue, facilitating Cys-adduct formation in the dark state (*SI Appendix*, Fig. S7 B and E).
239 However, DXCF CBCRs from the other lineages that retain this His residue have been shown
240 to retain the ability to form reversible Cys-adducts (8, 9, 11–13). This indicates that the role
241 of this Tyr residue for Cys-adduct formation is context dependent and may be restricted to
242 this specific lineage.

243

244 **A conserved Phe residue is critical for 15E photoproduct tuning.** Based on the blue–
245 shifted absorbance maxima of their ^{15E} photoproduct states, wild-type AM1_1499g1 and
246 S₁₁₈C, S₁₁₈C/Y₁₅₁L/T₁₅₉N, and S₁₁₈C/H₁₄₇Y variants likely possess chromophores with

247 twisted, out-of-plane D-ring conformations. A previous study concluded that two conserved
248 Phe residues in an α -helix and a β -sheet stabilize this twisted geometry to generate teal-
249 absorbing photoproducts (Fig. 1 B and C and *SI Appendix*, Fig. S2C–iii) (21). Since
250 AM1_1499g1 also possesses both Phe residues, we substituted these two residues with Val or
251 Leu to test their role in photoproduct spectral tuning. To do so, we used the blue/teal
252 S₁₁₈C/H₁₄₇Y background to yield the F₉₇V/S₁₁₈C/H₁₄₇Y and S₁₁₈C/H₁₄₇Y/F₁₅₄L triple mutants
253 (*SI Appendix*, Fig. S5 D and E). Spectral measurements showed that the F₉₇V replacement,
254 but not F₁₅₄L replacement, effectively converted the teal-absorbing photoproduct of the
255 parent to a green-absorbing one in F₉₇V/S₁₁₈C/H₁₄₇Y. Based on these results, we conclude
256 that the β -sheet Phe97 is a critical determinant for out-of-plane twisting of the D-ring.

257 To further test this hypothesis, we expressed the four variants F₉₇V, F₉₇V/S₁₁₈C,
258 F₉₇V/S₁₁₈C/Y₁₅₁L/T₁₅₉N, and F₉₇V/S₁₁₈C/H₁₄₇Y (*SI Appendix*, Fig. S3B), each of which
259 replaces the β -sheet Phe97 with a Val residue. The absorption spectra of these variants
260 indicated that the F₉₇V substitution had no influence on the ability of the parent construct to
261 isomerize PCB to PVB (Fig. 2 E–H, Table 1, and *SI Appendix*, Fig. S4 E–H and Table S1).
262 These analyses showed the F₉₇V variant possessed a PCB chromophore, while PVB
263 chromophores were present in all variants containing the S₁₁₈C substitution. Moreover, the
264 introduction of the F₉₇V mutation afforded red-shifted photoproduct states relative to those of
265 the parent constructs, while the dark state spectra of each variant were nearly
266 indistinguishable from those of their parents (Figs. 2 E–H, 3B, Table 1, and *SI Appendix*, Fig.
267 S4 E–H and Table S1).

268

269 **Thermochromism is lost in the AM1_1499g1 variants.** We next examined whether the
270 temperature dependency of the photoproduct spectrum of wild-type AM1_1499g1 was
271 present in the variant constructs described above (*SI Appendix*, Fig. S4A and Table S1).

272 Surprisingly, none of these variants exhibited thermochromic behavior in either photostate (*SI*
273 *Appendix*, Fig. S4 B–H and Table S1). As we described above, the thermochromic behavior
274 of wild-type AM1_1499g1 appears to be due to a temperature-dependent equilibrium
275 between a green-absorbing 15E Pg photoproduct with a twisted D-ring and a yellow-absorbing
276 15E Py photoproduct with a less constrained chromophore. In this context, it is reasonable that
277 the variant molecules possessing F₉₇V replacement did not show temperature effects, because
278 the F₉₇V replacement abolished the twisted geometry of the D-ring. All other variants
279 possessed covalently bound PVB. The twisted A-ring geometry observed in the 15E
280 photoproducts of red/green CBCRs (30, 31) cannot form with PVB because of the saturated
281 C5 methine bridge, which may disrupt this equilibrium.

282 To obtain further information on the D-ring conformation, we measured circular
283 dichroism (CD) spectra of these molecules in both states (*SI Appendix*, Fig. S8 A–H and
284 Table S2). All proteins showed negative CD in the visible region for both photostates,
285 including wild-type AM1_1499g1 at both low (5°C) and high (30°C) temperatures (*SI*
286 *Appendix*, Fig. S8I and Table S2). These results suggested that the D-ring is placed toward
287 the α -face relative to the C-ring plane irrespective of thermochromism (*SI Appendix*, Fig.
288 S8J) (32). The thermochromism of AM1_1499g1 thus does not arise from heterogeneous
289 facial dispositions of the bilin D-rings and may arise from some other form of heterogeneity.
290 Such heterogeneity is well established in other phytochrome and CBCR systems (31, 33, 34).

291

292 **CBCRs provide a useful toolbox of spectrally diverse photoswitches for optogenetic**
293 **applications based on a single protein scaffold.** Owing to their broad spectral diversity
294 from the near UV to the near IR and their small size, CBCRs have a bright future for
295 optogenetic tool development (2, 35). Through engineering of AM1_1499g1, we have
296 successfully developed a broad spectral arsenal of photoswitches - all based on a single

297 CBCR scaffold. The robust yellow/teal photocycle of the S₁₁₈C variant offers a large spectral
298 separation in photoproduct states (up to 90 nm) that is advantageous for strict optogenetic
299 control. In addition, this variant fills in a spectral gap in the current palette of photoswitches
300 that sense blue, green and red light, e.g. flavin-based photoreceptors (36–38), cobalamin-
301 based photoreceptors (39, 40), CBCRs (41, 42), and phytochromes (43–45).

302 As proof of concept, we chose to develop an optogenetic tool that leverages light to
303 reversibly modulate the level of cyclic adenosine monophosphate (cAMP). To do so, we
304 constructed a fusion protein between AM1_1499g1_S₁₁₈C and the catalytic region of CyaB1,
305 an adenylate cyclase (AC) from cyanobacterium *Anabaena* sp. PCC 7120 (*SI Appendix*, Fig.
306 S9A) (46). The S₁₁₈C-AC chimera exhibited a robust yellow/teal photocycle indistinguishable
307 from that of the S₁₁₈C variant on its own (*SI Appendix*, Fig. S9 B and C). We measured the
308 time course of AC activity of both forms by quantitating cAMP levels produced via HPLC
309 analysis (*SI Appendix*, Fig. S9D). The ^{15Z}Py form showed about five times higher AC activity
310 than the ^{15E}Pt form (Fig. 4 and *SI Appendix*, Table S3), establishing a proof-of-concept design
311 principle for a new family of light-regulated cAMP optogenetic probes based on the
312 AM1_1499g1 scaffold. It should thus be possible to develop an entire family of light-
313 responsive adenylate cyclases with different color responses using a single AM1_1499g1
314 chimera with well-chosen site-directed mutagenesis rather than by laborious optimization of
315 multiple chimeras.

316

317 **Conclusions and Future Perspective.** We show that AM1_1499g1 is a PCB-containing
318 CBCR that lacks a 2nd Cys and cannot isomerize PCB to PVB. Via structure- and sequence-
319 informed mutagenesis that introduced PCB-to-PVB isomerization activity, 2nd-linkage
320 formation, and out-of-plane trapped-twist of the bilin D-ring, we generated seven variants
321 that exhibit robust yellow/teal, green/teal, blue/teal, yellow/orange, yellow/green, green/green,

322 and blue/green photocycles. We also leveraged one of the variant molecules to generate a
323 chimeric molecule that reversibly regulates cAMP production under yellow and teal light. In
324 the future, we hope to introduce mutations that were successful in altering the chromophore
325 specificity of the red/green CBCR sensor AnPixJg2 (47), enabling substitution of PCB with
326 biliverdin IX α , a much more widespread bilin than PCB. In principle, the lessons learned
327 from such studies could prove useful for generation of an unprecedented palette of
328 photoswitches based on the AM1_1499g1 scaffold for novel optogenetic applications in
329 mammalian cells.
330

331 **Materials and Methods**

332 **Bacterial strains and growth media.** The *Escherichia coli* strain JM109 (TaKaRa) was used
333 for cloning plasmid DNA and *E. coli* strain C41 (Cosmo Bio) harboring PCB synthetic
334 systems, pKT271, was used for protein expression as previously reported (48). Bacterial cells
335 were grown in Lysogeny Broth (LB) medium containing 20 $\mu\text{g mL}^{-1}$ kanamycin with or
336 without 20 $\mu\text{g mL}^{-1}$ chloramphenicol. For protein expression, cells were grown in LB
337 containing the appropriate antibiotic(s) at 37°C until the optical density at 600 nm was 0.4–
338 0.8. Isopropyl β -D-1-thiogalactopyranoside (IPTG) then was added to a final concentration of
339 0.1 mM and cells were cultured at 18°C overnight.

340 **Bioinformatic analyses.** Multiple sequence alignment and neighbor-joining phylogenetic
341 trees were constructed with MEGA7 software (49). The crystal structures of PVB-bound
342 TePixJg (^{15}Z Pb form, PDB_ID: 4GLQ; ^{15}E Pg form, PDB_ID: 3VV4) were utilized to assess
343 key amino acid residues for color-tuning. Molecular graphics were generated by UCSF
344 Chimera software (50).

345 **Plasmid construction.** Plasmids expressing His-tagged AM1_1499g1 (amino acid positions
346 47–222) and Npr5113g3 (amino acid positions 388–557) (11, 15, 21) were amplified by
347 PCR from *Acaryochloris marina* MBIC11017 and *Nostoc punctiforme* PCC 73102 genomic
348 DNA, respectively, using PrimeSTAR Max DNA polymerase (TaKaRa) and the appropriate
349 nucleotide primers (*SI Appendix*, Table S4). AM1_6305g1 (amino acid positions 33–203) (8)
350 was constructed as described in previous studies. The Gibson Assembly System (New
351 England Biolabs, Japan) was used to fuse the cloned DNA fragments into the pET28a
352 expression vector. The PrimeSTAR Max Basal Mutagenesis kit reagents (TaKaRa) or KOD
353 One PCR Master Mix (Toyobo Life Science) with appropriate nucleotide primers were used
354 to perform site-directed mutagenesis of these proteins (*SI Appendix*, Table S4). All the
355 expression constructs were verified by nucleotide sequencing (FASMAC).

356 **Protein purification.** All the proteins were expressed in *E. coli* C41 containing the bilin
357 biosynthetic plasmid pKT271 in 1 L LB. After expression, cells were disrupted in lysis buffer
358 (20 mM HEPES-NaOH pH 7.5, 0.1 M NaCl and 10% (w/v) glycerol with or without 0.5 mM
359 Tris(2-carboxyethyl)phosphine) using three passages through an Emulsiflex C5 high-pressure
360 homogenizer at 12,000 psi (Avestin). Homogenates were centrifuged at 165,000 g for 30 min
361 and supernatants were filtered through a 0.8 µm cellulose acetate membrane before loading
362 onto a nickel-affinity His-trap column (GE Healthcare) using an ÄKTAprime plus (GE
363 Healthcare) System. The column was washed with Lysis Buffer containing 100 mM
364 imidazole to remove unbound proteins and His-tagged proteins subsequently were eluted
365 with a linear gradient of Lysis Buffer containing 100 to 400 mM imidazole (1 mL/min, total
366 15 min). After incubation with 1 mM EDTA for 1 hour on ice, purified proteins were
367 dialyzed against lysis buffer with or without 1 mM dithiothreitol (DTT) to remove EDTA and
368 imidazole. Protein concentrations were determined by the Bradford method.

369 **Electrophoresis and fluorescence detection.** Purified proteins were diluted into 60 mM
370 Tris-HCl pH 8.0, 2% (w/v) SDS and 60 mM DTT, denatured at 95°C for 3 min, and
371 electrophoresed at room temperature (r.t.) using 12% (w/v) SDS polyacrylamide gels. The
372 electrophoresed gels were soaked in distilled water for 30 min followed by visualizing
373 fluorescence bands (details for detection of the fluorescence were described in previous
374 studies) (46, 47), and then were stained with Coomassie Brilliant Blue R-250 (CBB).

375 **Spectroscopy.** Ultraviolet and visible absorption spectra of the proteins were recorded with a
376 UV-2600 spectrophotometer (SHIMADZU) at ambient temperature. AM1_1499g1 and its
377 variant proteins were also measured at 5 and 30°C, using a thermostatted cuvette holder.
378 Circular dichroism spectra of AM1_1499g1 and its variant proteins were recorded with a J-
379 820 spectrophotometer (JASCO) at ambient temperature. Wild-type AM1_1499g1 was
380 measured additionally at 5 and 30°C, using a thermostatted cuvette holder. An Opto-

381 Spectrum Generator (Hamamatsu Photonics, Inc.) was used to generate monochromatic light
382 of various wavelengths to induce photoconversion: Pb form, 400–430 nm; Pt form, 470–490
383 nm; Pg form, 470–620 nm; Py form, 490–640 nm; Po form, 600–640 nm.

384 **Biochemical characterization of cyanobacteriochromes.** For denaturation assays, both
385 dark state (*15Z*-isomer) and photoproduct state (*15E*-isomer) of the native proteins obtained
386 at 5 or 30°C were 5-fold diluted into acidic 8 M urea <pH 2.0 and their absorption spectra
387 were recorded at ambient temperature before and after 3 min of illumination with white light.
388 To assign the spectral peaks to the chromophore incorporated into each protein, those of
389 known PCB- and PVB-binding CBCRs were recorded under the same conditions.

390 **Light-dependent enzymatic reaction of adenylate cyclase.** The chimeric protein,
391 AM1_1499g1_S₁₁₈C-AC, was constructed using the method in a previous study (46) (*SI*
392 *Appendix*, Fig. S9A). The concentration of the purified protein was calculated using the
393 Bradford method (Bio-Rad) using bovine serum albumin as a protein standard. After
394 photoconversion to ^{15Z}Py and ^{15E}Pt forms with saturating monochromatic light, the chimeric
395 protein (in lysis buffer; 20 mM HEPES-NaOH pH 7.5, 0.1 M NaCl and 10% (w/v) glycerol
396 with 1 mM DTT) was added to a reaction buffer containing ATP. The final concentrations of
397 each component in the reaction mixture was as follows: 1 μM chimeric protein, 100 μM ATP,
398 50 mM Tris-HCl (pH 8.0), 50 mM NaCl, 10 mM MgCl₂. Enzymatic reactions were
399 performed at 25°C under teal or yellow light irradiation. Aliquots were removed after 0, 5, 10,
400 20, 30, and 60 min, and the reaction was stopped by heating at 95°C for 3 min. As an internal
401 standard, nicotine adenosine dinucleotide (NAD) was added to all samples and adjusted to 1
402 mM as final concentration. After centrifugation, supernatants were filtered through a 0.2 μm
403 PTFE membrane to remove insoluble aggregates. NAD, produced cAMP and ATP in the
404 samples were detected using a Prominence HPLC system (SHIMADZU) with a reverse-
405 phase HPLC column (Kinetex C18, 2.1 i.d. x 100 mm, 1.7 μm; Phenomenex) and eluted with

406 a linear gradient of MeOH and phosphate buffer as described in a previous study (46). Each
407 sample (20 μ L) was injected and absorbance at 260 nm was monitored. Quantities of
408 accumulated cAMP by the enzymatic reaction were calculated from the ratio of the peak area
409 of cAMP to that of NAD using standard curves. Nucleotides were assigned based on their
410 retention times (t_R) of standard compounds.

411

412 **Data Availability**

413 In this study, we did not obtain any sequence and structural data to deposit in community-
414 approved public repositories. We used sequence and structural information of
415 cyanobacteriochromes (CBCRs) already deposited in the public repositories, such as National
416 Center for Biotechnology Information (NCBI) and Protein Data Bank (PDB), for *in silico*
417 analysis.

418

419 **Acknowledgments**

420 We thank Shelley S. Martin (University of California, Davis) for the gift of the plasmid
421 constructs. We thank Prof. Masayuki Yazawa (Columbia University) for helpful discussion.
422 We thank Mr. Tatsuki Masuzawa, Prof. Takanori Oyoshi and Prof. Mitsuru Kondo (Shizuoka
423 University) for experimental assistance. This work was supported by grants from JST,
424 CREST (JPMJCR1653 to M.I. and R.N.), from JSPS KAKENHI (26702036 to R.N.) and
425 from the Chemical Sciences, Geosciences, and Biosciences Division, Office of Basic Energy
426 Sciences, Office of Science, United States Department of Energy (DOE DE-FG02-
427 09ER16117 to J.C.L.).

428

429

430 **References**

- 431 1. M. Ikeuchi, T. Ishizuka, Cyanobacteriochromes: a new superfamily of tetrapyrrole-
432 binding photoreceptors in cyanobacteria. *Photochem. Photobiol. Sci.* **7**, 1159–1167
433 (2008).
- 434 2. K. Fushimi, R. Narikawa, Cyanobacteriochromes: photoreceptors covering the entire
435 UV-to-visible spectrum. *Curr. Opin. Struct. Biol.* **57**, 39–46 (2019).
- 436 3. N. C. Rockwell, J. C. Lagarias, Phytochrome evolution in 3D: deletion, duplication, and
437 diversification. *New Phytol.* (2019) <https://doi.org/10.1111/nph.16240>.
- 438 4. L.-O. Essen, J. Mailliet, J. Hughes, The structure of a complete phytochrome sensory
439 module in the Pr ground state. *Proc. Natl. Acad. Sci. U. S. A.* **105**, 14709–14714 (2008).
- 440 5. N. C. Rockwell, *et al.*, A second conserved GAF domain cysteine is required for the
441 blue/green photoreversibility of cyanobacteriochrome Tlr0924 from
442 *Thermosynechococcus elongatus*. *Biochemistry* **47**, 7304–7316 (2008).
- 443 6. N. C. Rockwell, S. S. Martin, K. Feoktistova, J. C. Lagarias, Diverse two-cysteine
444 photocycles in phytochromes and cyanobacteriochromes. *Proc. Natl. Acad. Sci. U. S. A.*
445 **108**, 11854–11859 (2011).
- 446 7. T. Ishizuka, *et al.*, The cyanobacteriochrome, TePixJ, isomerizes its own chromophore
447 by converting phycocyanobilin to phycoviolobilin. *Biochemistry* **50**, 953–961 (2011).
- 448 8. M. Hasegawa, *et al.*, Molecular characterization of DXCF cyanobacteriochromes from
449 the cyanobacterium *Acaryochloris marina* identifies a blue-light power sensor. *J. Biol.*
450 *Chem.* **293**, 1713–1727 (2018).
- 451 9. Q. Ma, *et al.*, A rising tide of blue-absorbing biliprotein photoreceptors: characterization
452 of seven such bilin-binding GAF domains in *Nostoc* sp. PCC7120. *FEBS J.* **279**, 4095–
453 4108 (2012).
- 454 10. S. M. Cho, *et al.*, Genomic survey and biochemical analysis of recombinant candidate
455 cyanobacteriochromes reveals enrichment for near UV/violet sensors in the halotolerant
456 and alkaliphilic cyanobacterium *Microcoleus* IPPAS B353. *J. Biol. Chem.* **290**, 28502–
457 28514 (2015).
- 458 11. N. C. Rockwell, S. S. Martin, A. G. Gulevich, J. C. Lagarias, Phycoviolobilin formation
459 and spectral tuning in the DXCF cyanobacteriochrome subfamily. *Biochemistry* **51**,
460 1449–1463 (2012).
- 461 12. S. Yoshihara, M. Katayama, X. Geng, M. Ikeuchi, Cyanobacterial phytochrome-like
462 PixJ1 holoprotein shows novel reversible photoconversion between blue- and green-
463 absorbing forms. *Plant Cell Physiol.* **45**, 1729–1737 (2004).
- 464 13. T. Ishizuka, *et al.*, Characterization of cyanobacteriochrome TePixJ from a thermophilic
465 cyanobacterium *Thermosynechococcus elongatus* strain BP-1. *Plant Cell Physiol.* **47**,
466 1251–1261 (2006).
- 467 14. T. Ishizuka, R. Narikawa, T. Kohchi, M. Katayama, M. Ikeuchi, Cyanobacteriochrome

- 468 TePixJ of *Thermosynechococcus elongatus* harbors phycoviolobin as a chromophore.
469 *Plant Cell Physiol.* **48**, 1385–1390 (2007).
- 470 15. N. C. Rockwell, S. S. Martin, J. C. Lagarias, Mechanistic insight into the photosensory
471 versatility of DXCF cyanobacteriochromes. *Biochemistry* **51**, 3576–3585 (2012).
- 472 16. R. Narikawa, *et al.*, Structures of cyanobacteriochromes from phototaxis regulators
473 AnPixJ and TePixJ reveal general and specific photoconversion mechanism. *Proc. Natl.*
474 *Acad. Sci. U. S. A.* **110**, 918–923 (2013).
- 475 17. E. S. Burgie, J. M. Walker, G. N. Phillips Jr, R. D. Vierstra, A photo-labile thioether
476 linkage to phycoviolobin provides the foundation for the blue/green photocycles in
477 DXCF-cyanobacteriochromes. *Structure* **21**, 88–97 (2013).
- 478 18. C. C. Cornilescu, *et al.*, Dynamic structural changes underpin photoconversion of a
479 blue/green cyanobacteriochrome between its dark and photoactivated states. *J. Biol.*
480 *Chem.* **289**, 3055–3065 (2014).
- 481 19. L. B. Wiltbank, D. M. Kehoe, Two cyanobacterial photoreceptors regulate
482 photosynthetic light harvesting by sensing teal, green, yellow, and red light. *MBio* **7**,
483 e02130–15 (2016).
- 484 20. N. C. Rockwell, S. S. Martin, J. C. Lagarias, Identification of DXCF
485 cyanobacteriochrome lineages with predictable photocycles. *Photochem. Photobiol. Sci.*
486 **14**, 929–941 (2015).
- 487 21. N. C. Rockwell, S. S. Martin, A. G. Gulevich, J. C. Lagarias, Conserved phenylalanine
488 residues are required for blue-shifting of cyanobacteriochrome photoproducts.
489 *Biochemistry* **53**, 3118–3130 (2014).
- 490 22. R. Narikawa, G. Enomoto, Ni-Ni-Win, K. Fushimi, M. Ikeuchi, A new type of dual-Cys
491 cyanobacteriochrome GAF domain found in cyanobacterium *Acaryochloris marina*,
492 which has an unusual red/blue reversible photoconversion cycle. *Biochemistry* **53**, 5051–
493 5059 (2014).
- 494 23. R. Narikawa, *et al.*, A biliverdin-binding cyanobacteriochrome from the chlorophyll *d*-
495 bearing cyanobacterium *Acaryochloris marina*. *Sci. Rep.* **5**, 7950 (2015).
- 496 24. R. Narikawa, K. Fushimi, Ni-Ni-Win, M. Ikeuchi, Red-shifted red/green-type
497 cyanobacteriochrome AM1_1870g3 from the chlorophyll *d*-bearing cyanobacterium
498 *Acaryochloris marina*. *Biochem. Biophys. Res. Commun.* **461**, 390–395 (2015).
- 499 25. K. Fushimi, *et al.*, Photoconversion and fluorescence properties of a red/green-type
500 cyanobacteriochrome AM1_C0023g2 that binds not only phycocyanobilin but also
501 biliverdin. *Front. Microbiol.* **7**, 588 (2016).
- 502 26. N. C. Rockwell, S. S. Martin, S. Lim, J. C. Lagarias, J. B. Ames, Characterization of
503 red/green cyanobacteriochrome NpR6012g4 by solution nuclear magnetic resonance
504 spectroscopy: A protonated bilin ring system in both photostates. *Biochemistry* **54**,
505 2581–2600 (2015).
- 506 27. N. C. Rockwell, S. S. Martin, S. Lim, J. C. Lagarias, J. B. Ames, Characterization of

- 507 red/green cyanobacteriochrome NpR6012g4 by solution nuclear magnetic resonance
508 spectroscopy: A hydrophobic pocket for the C15-*E,anti* chromophore in the
509 photoproduct. *Biochemistry* **54**, 3772–3783 (2015).
- 510 28. P. W. Kim, N. C. Rockwell, S. S. Martin, J. C. Lagarias, D. S. Larsen, Dynamic
511 inhomogeneity in the photodynamics of cyanobacterial phytochrome Cph1.
512 *Biochemistry* **53**, 2818–2826 (2014).
- 513 29. J. R. Wagner, J. S. Brunzelle, K. T. Forest, R. D. Vierstra, A light-sensing knot revealed
514 by the structure of the chromophore-binding domain of phytochrome. *Nature* **438**, 325–
515 331 (2005).
- 516 30. X. Xu, *et al.*, Structural elements regulating the photochromicity in a
517 cyanobacteriochrome. *Proc. Natl. Acad. Sci. U. S. A.* (2020)
518 <https://doi.org/10.1073/pnas.1910208117>.
- 519 31. S. Lim, *et al.*, Correlating structural and photochemical heterogeneity in
520 cyanobacteriochrome NpR6012g4. *Proc. Natl. Acad. Sci. U. S. A.* **115**, 4387–4392
521 (2018).
- 522 32. N. C. Rockwell, L. Shang, S. S. Martin, J. C. Lagarias, Distinct classes of red/far-red
523 photochemistry within the phytochrome superfamily. *Proc. Natl. Acad. Sci. U. S. A.* **106**,
524 6123–6127 (2009).
- 525 33. C. Song, *et al.*, Two ground state isoforms and a chromophore D-ring photoflip
526 triggering extensive intramolecular changes in a canonical phytochrome. *Proc. Natl.*
527 *Acad. Sci. U. S. A.* **108**, 3842–3847 (2011).
- 528 34. F. Velazquez Escobar, *et al.*, Protonation-dependent structural heterogeneity in the
529 chromophore binding site of cyanobacterial phytochrome Cph1. *J. Phys. Chem. B* **121**,
530 47–57 (2017).
- 531 35. T. Ziegler, A. Möglich, Photoreceptor engineering. *Front Mol Biosci* **2**, 30 (2015).
- 532 36. M. Yazawa, A. M. Sadaghiani, B. Hsueh, R. E. Dolmetsch, Induction of protein-protein
533 interactions in live cells using light. *Nat. Biotechnol.* **27**, 941–945 (2009).
- 534 37. M. J. Kennedy, *et al.*, Rapid blue-light-mediated induction of protein interactions in
535 living cells. *Nat. Methods* **7**, 973–975 (2010).
- 536 38. F. Kawano, H. Suzuki, A. Furuya, M. Sato, Engineered pairs of distinct photoswitches
537 for optogenetic control of cellular proteins. *Nat. Commun.* **6**, 6256 (2015).
- 538 39. S. Kainrath, M. Stadler, E. Reichhart, M. Distel, H. Janovjak, Green-light-induced
539 inactivation of receptor signaling using cobalamin-binding domains. *Angew. Chem. Int.*
540 *Ed Engl.* **56**, 4608–4611 (2017).
- 541 40. C. Chatelle, *et al.*, A green-light-responsive system for the control of transgene
542 expression in mammalian and plant cells. *ACS Synth. Biol.* **7**, 1349–1358 (2018).
- 543 41. J. J. Tabor, A. Levskaya, C. A. Voigt, Multichromatic control of gene expression in
544 *Escherichia coli*. *J. Mol. Biol.* **405**, 315–324 (2011).

- 545 42. S. Senoo, S. T. Tandar, S. Kitamura, Y. Toya, H. Shimizu, Light-inducible flux control
546 of triosephosphate isomerase on glycolysis in *Escherichia coli*. *Biotechnol. Bioeng.*
547 (2019) <https://doi.org/10.1002/bit.27148>.
- 548 43. S. Shimizu-Sato, E. Huq, J. M. Tepperman, P. H. Quail, A light-switchable gene
549 promoter system. *Nat. Biotechnol.* **20**, 1041–1044 (2002).
- 550 44. A. Levskaya, O. D. Weiner, W. A. Lim, C. A. Voigt, Spatiotemporal control of cell
551 signalling using a light-switchable protein interaction. *Nature* **461**, 997–1001 (2009).
- 552 45. E. Reichhart, A. Ingles-Prieto, A.-M. Tichy, C. McKenzie, H. Janovjak, A phytochrome
553 sensory domain permits receptor activation by red light. *Angew. Chem. Int. Ed Engl.* **55**,
554 6339–6342 (2016).
- 555 46. K. Fushimi, G. Enomoto, M. Ikeuchi, R. Narikawa, Distinctive properties of dark
556 reversion kinetics between two red/green-type cyanobacteriochromes and their
557 application in the photoregulation of cAMP synthesis. *Photochem. Photobiol.* **93**, 681–
558 691 (2017).
- 559 47. K. Fushimi, *et al.*, Rational conversion of chromophore selectivity of
560 cyanobacteriochromes to accept mammalian intrinsic biliverdin. *Proc. Natl. Acad. Sci.*
561 *U. S. A.* **116**, 8301–8309 (2019).
- 562 48. K. Mukougawa, H. Kanamoto, T. Kobayashi, A. Yokota, T. Kohchi, Metabolic
563 engineering to produce phytochromes with phytochromobilin, phycocyanobilin, or
564 phycoerythrobilin chromophore in *Escherichia coli*. *FEBS Lett.* **580**, 1333–1338 (2006).
- 565 49. S. Kumar, G. Stecher, K. Tamura, MEGA7: Molecular evolutionary genetics analysis
566 version 7.0 for bigger datasets. *Mol. Biol. Evol.* **33**, 1870–1874 (2016).
- 567 50. E. F. Pettersen, *et al.*, UCSF Chimera--a visualization system for exploratory research
568 and analysis. *J. Comput. Chem.* **25**, 1605–1612 (2004).
- 569
- 570

571 **Table**

572 **Table 1. Spectral properties of AM1_1499g1 and its variant proteins.**

	Bilin pigment	Dark state	Photoproduct state	Dark – Photoproduct	
		(Z-isomer)	(E-isomer)	Positive (nm)	Negative (nm)
		λ_{\max} (nm)	λ_{\max} (nm)		
WT	PCB	613	544	623	536
S₁₁₈C	PVB	577	491	577	491
S₁₁₈C/Y₁₅₁L/T₁₅₉N	PVB	559	492	561	492
S₁₁₈C/H₁₄₇Y	PVB	414	492	414	492
F₉₇V	PCB	620	585	637	521
F₉₇V/S₁₁₈C	PVB	577	514	578	505
F₉₇V/S₁₁₈C/Y₁₅₁L/T₁₅₉N	PVB	560	524	566	507
F₉₇V/S₁₁₈C/H₁₄₇Y	PVB	414	511	418	512

573

574 Absorption spectra of the WT protein were measured at low (5°C) temperature whereas those

575 of its variant proteins were measured at room temperature.

576 Difference spectra (15Z dark state – 15E photoproduct state) of their proteins were obtained

577 from their absorption spectra.

578 PCB, phycocyanobilin, PVB, phycoviolobilin.

579 **Figure Legends**

580 **Figure 1. Photochemical diversity of CBCRs.** Crystal structures of DXCF CBCR TePixJ in
581 the ^{15Z}Pb form (A: PDB_ID: 4GLQ; amino acid residues, cyan; chromophore, gray) and the
582 ^{15E}Pg form (B: 4GLQ; amino acid residues, lime green; chromophore, gray). Key mutation
583 sites Val473, Cys494 of the 2nd Cys, His523, Leu527, Leu530, and Asn535 in TePixJg (Te)
584 are shown, corresponding to residues Phe97, Ser118, His147, Tyr151, Phe154, and Thr159 in
585 AM1_1499g1 (AM). These amino acid residues are highlighted in a sequence shown below.
586 (C) Sequence comparison between AM1_1499g1 (orange), green/teal (yellow green),
587 blue/teal (blue) and blue/green (violet) CBCRs. Predicted secondary structures of the ^{15Z}Pb
588 (cyan) and the ^{15E}Pg (lime green) forms and amino acid residues within 6 Å of the
589 chromophores (asterisks) are based on the structures of the ^{15Z}Pb form of TePixJg (PDB_ID:
590 4GLQ) and the ^{15E}Pg form of TePixJg (PDB_ID: 3VV4). Amino acid residues of
591 AM1_1499g1 mutated in this study (shown in sky blue) were substituted with residues found
592 in other CBCRs (shown in orange). Highly conserved residues shown in black boldface type
593 include the nearly invariant 1st Cys and the 2nd Cys found in Asp-Xaa-Cys-Phe (DXCF)
594 motif. (D) Phylogenetic tree of selected CBCRs and phytochromes, based on the alignment
595 shown in the *SI Appendix*, Supplementary Data file. Each lineage ‘cluster’ is classified
596 according to photocycle. CBCR subfamilies possessing the DXCF motif are indicated with
597 asterisks.

598

599 **Figure 2. Photocycles of AM1_1499g1 variants.** (A–H) Normalized absorption spectra of
600 AM1_1499g1 and variants are depicted with structures for each chromophore. The π -
601 conjugated systems for each bilin are color-coded by dark state peak absorption wavelength.
602 (A) Wild-type AM1_1499g1 incorporates PCB and exhibits an orange/green photocycle at
603 low (5°C) temperature. (B) The S₁₁₈C variant incorporates PVB and exhibits a yellow/teal

604 photocycle. (C) The S₁₁₈C/Y₁₅₁L/T₁₅₉N variant incorporates PVB and exhibits a green/teal
605 photocycle. (D) The S₁₁₈C/H₁₄₇Y variant incorporates PVB and exhibits a blue/teal
606 photocycle. (E) The F₉₇V variant incorporates PCB and exhibits an orange/yellow photocycle.
607 (F) The F₉₇V/S₁₁₈C variant incorporates PVB and exhibits a yellow/green photocycle. (G)
608 The F₉₇V/S₁₁₈C/Y₁₅₁L/T₁₅₉N variant incorporates PVB and exhibits a green/green photocycle.
609 (H) The F₉₇V/S₁₁₈C/H₁₄₇Y variant incorporates PVB and exhibits a blue/green photocycle.
610 Absorption maxima are reported in Table 1. Some samples, especially the F₉₇V/S₁₁₈C/H₁₄₇Y
611 variant, showed higher absorption in the shorter wavelength region due to scattering,
612 indicating that these samples are unstable in solution.

613

614 **Figure 3. Comparative photochemical difference spectra of wild-type AM1-1499g1 and**
615 **its variants.** Normalized difference spectra (^{15Z} dark state – ^{15E} photoproduct state) are
616 shown for variants with twisted (A) or relaxed (B) D-ring photoproducts. (A) wild-type
617 AM1_1499g1 (^{15Z}Po – ^{15E}Pg, orange), S₁₁₈C (^{15Z}Py – ^{15E}Pt, yellow), S₁₁₈C/Y₁₅₁L/T₁₅₉N (^{15Z}Pg
618 – ^{15E}Pt, yellow green) and S₁₁₈C/H₁₄₇Y (^{15Z}Pb – ^{15E}Pt, blue). (B) F₉₇V (^{15Z}Po – ^{15E}Py, orange),
619 F₉₇V/S₁₁₈C (^{15Z}Py – ^{15E}Pg, yellow), F₉₇V/S₁₁₈C/Y₁₅₁L/T₁₅₉N (^{15Z}Pg – ^{15E}Pg, yellow green),
620 and F₉₇V/S₁₁₈C/H₁₄₇Y (^{15Z}Pb – ^{15E}Pg, blue). Absorption maxima are reported in Table 1.

621

622 **Figure 4. Light-dependent adenylylase activities of both photostates of**
623 **AM1_1499g1_S₁₁₈C-AC.** The enzymatic reaction catalyzing cAMP synthesis from ATP by
624 the AM1_1499g1_S₁₁₈C-adenylylase chimeric protein was examined after 0, 5, 10, 20,
625 30 and 60 min at 25°C for ^{15Z}Py (yellow) and ^{15E}Pt (teal). Reaction products were quantified
626 using HPLC (*SI Appendix*, Fig. S9D and Table S3). Data are reported as mean ± standard
627 deviation, calculated from three independent experiments.

628

Fig. 1

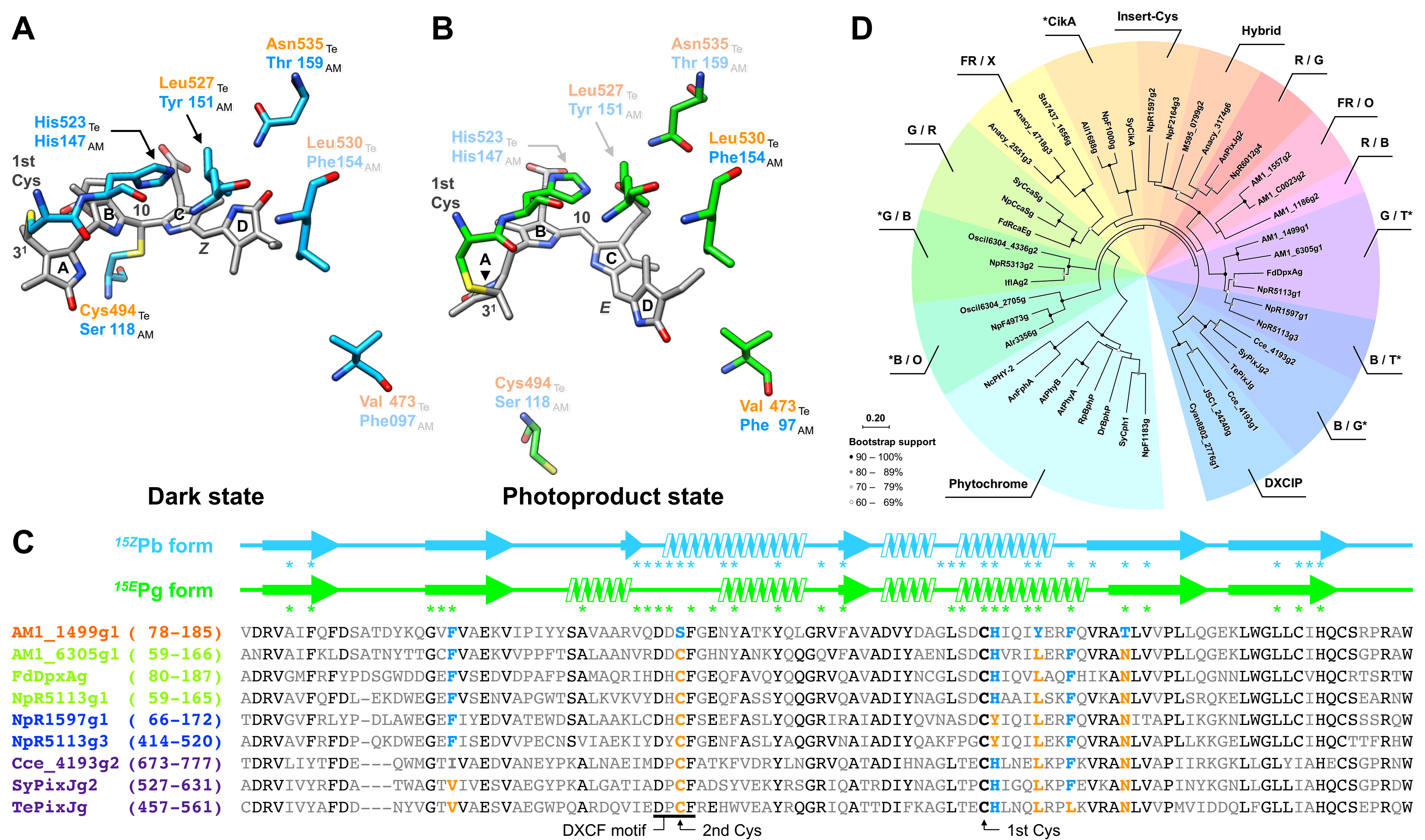


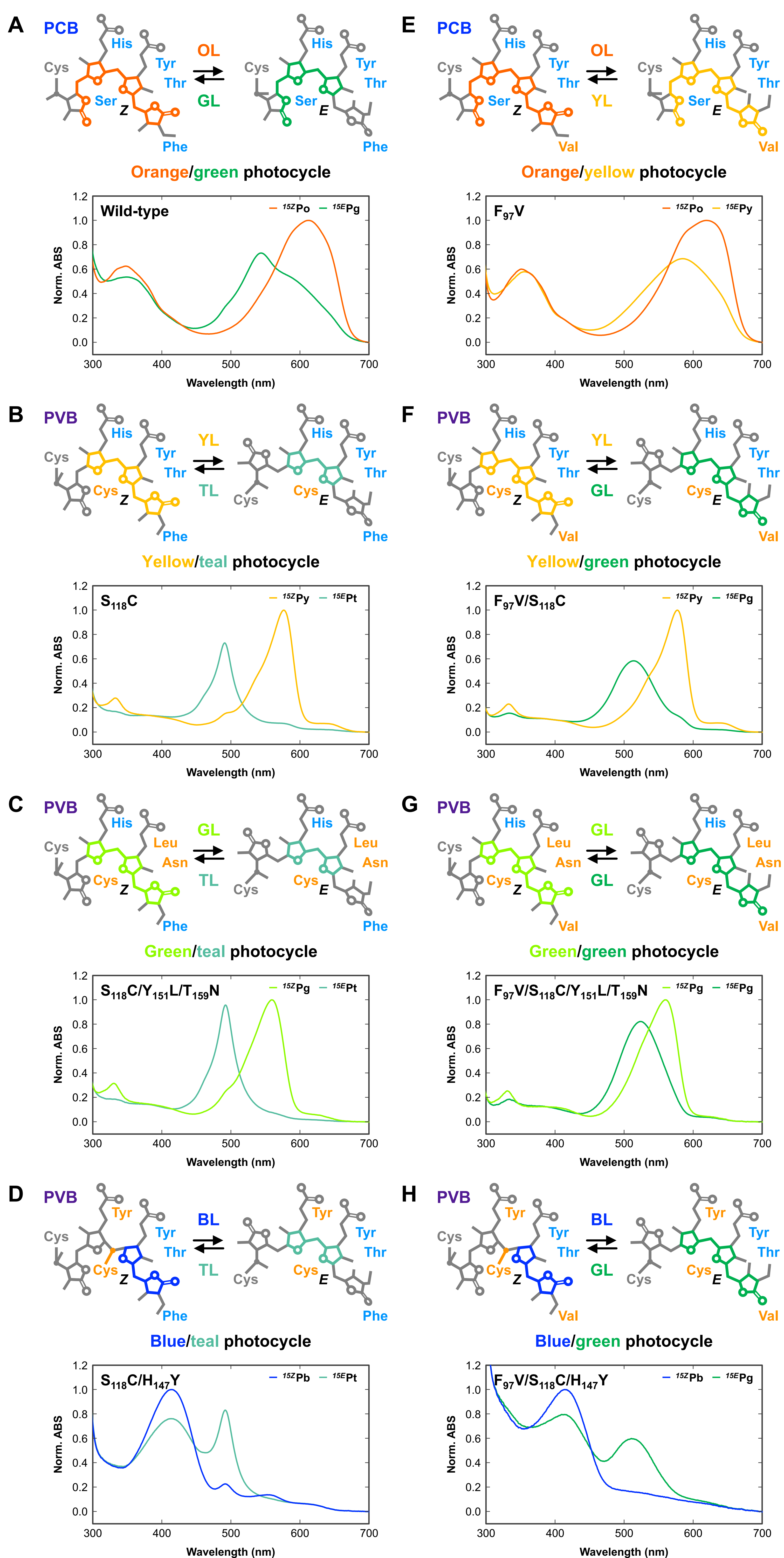
Fig. 2

Fig. 3

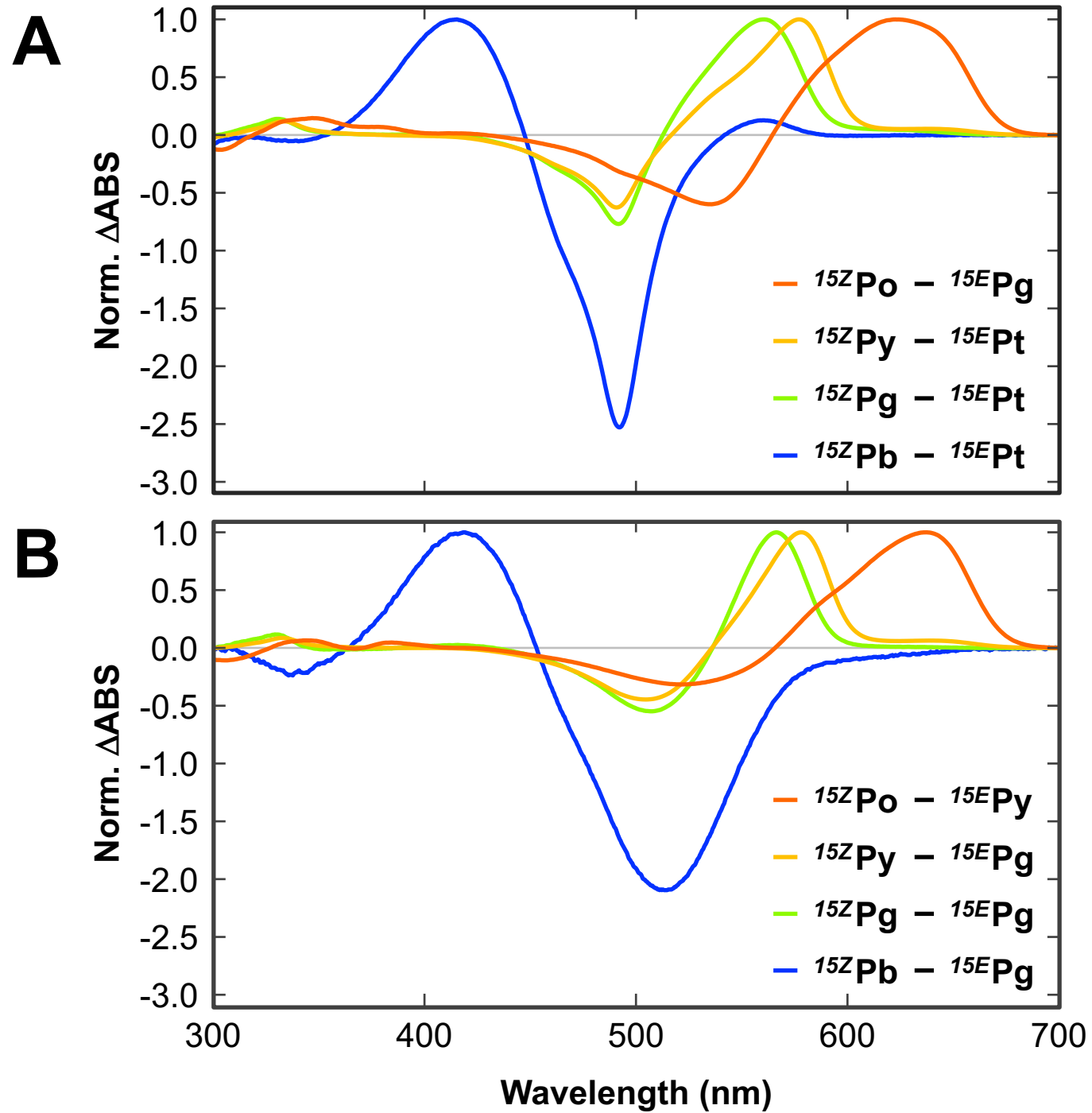


Fig. 4

